Measurement of the electric polarizability of ^{3}He

F. Goeckner, L. O. Lamm, and L. D. Knutson
Department of Physics, University of Wisconsin, Madison, Wisconsin 53706
(Received 30 July 1990)

Measurements of relative differential cross sections have been obtained for elastic scattering of ^{3}He nuclei from ^{208}Pb at energies well below the Coulomb barrier. The measurements show deviations from Rutherford scattering, which are attributed to electric polarization of the ^{3}He nuclei in the Coulomb field of ^{208}Pb. The deduced value of the electric polarizability for ^{3}He is $\alpha=0.250\pm0.040$ fm^3. This result is significantly larger than expected from measurements of cross sections for ^{3}He photodisintegration.

I. INTRODUCTION

The cross section for the scattering of nuclei at energies below the Coulomb barrier is given only approximately by the Rutherford formula. Even at energies low enough so that the effects of strong interactions between the two nuclei can be neglected, deviations may arise from several sources. One of the most important of these is the electric polarization of each nucleus by the Coulomb field of the other. It was first suggested by Bauer *et al.*[1] that one might be able to determine the electric polarizability of a nucleus by measuring deviations from Rutherford scattering at low energies. The practicality of this method was first demonstrated in the experiments of Lynch *et al.*[2] and the method has previously been used to measure the electric polarizability of the deuteron.[3] A similar approach has been used by Vetterli *et al.*[4] to observe effects of vacuum polarization in nuclear scattering.

In this paper we report an experiment in which this same technique was used to make the first experimental determination of the electric polarizability of the ^{3}He nucleus. Our primary interest in measuring this quantity is that it is a fundamental property of ^{3}He which, until now, had not been directly measured. However, it should be noted that the polarizability can be expressed in terms of an energy-weighted integral of the electric dipole photoabsorption cross section.[1,5] Since these cross sections have been measured, a comparison with previous experimental work is possible.

The method we use to determine the polarizability is described in Sec. II. The experimental details are given in Sec. III and the determination of the polarizability is described in Sec. IV. Finally, in Sec. V we compare the experimental result with expectations based on the photoabsorption sum rule.

II. METHOD

A nucleus which is located in a strong electric field **E** will become electrically polarized. If we consider only the induced dipole moment **P** the resulting polarization potential will be given by

$$V_{\rm pol}=-\tfrac{1}{2}\mathbf{P}\cdot\mathbf{E}\ . \tag{1}$$

For a static field, the induced moment is expected to be proportional to **E**; i.e.,

$$\mathbf{P}=\alpha\mathbf{E}\ , \tag{2}$$

where the constant α is the electric polarizability of the nucleus.

For the case of a ^{3}He nucleus passing near a heavy nucleus, the electric field seen by the ^{3}He is time dependent. However, for low bombarding energies the internal motion of the ^{3}He is much faster than the relative motion between the two nuclei. It is therefore reasonable to assume that the static field result, Eq. (2), holds at each point along the trajectory. This is referred to as the adiabatic approximation. In this case the polarization potential becomes

$$V_{\rm pol}=-\tfrac{1}{2}\alpha\frac{Z^2e^2}{R^4}\ , \tag{3}$$

where Ze is the charge of the target nucleus, and R is the distance between the two nuclei.

For reasonable values of α, the polarization potential is small compared to the ordinary Coulomb potential, $V_{\rm Coul}=zZe^2/R$, and can be treated as a perturbation. Thus we expect that the electric polarizability of the ^{3}He nucleus will give rise to deviations from Rutherford scattering that are proportional to α.

The electric polarizability has been measured by scattering ^{3}He nuclei from ^{208}Pb for bombarding energies ranging from 7 to 17 MeV. Because the deviations from Rutherford scattering are very small, direct measurement of the absolute cross section is impractical. Instead, we have adopted the method of Refs. 2 and 3 in which one measures a ratio of cross sections

$$R(E,\theta)=\frac{\sigma(E,\theta)}{\sigma(E,\theta_{\rm ref})}\Big/\frac{\sigma(E_{\rm ref},\theta)}{\sigma(E_{\rm ref},\theta_{\rm ref})}\ , \tag{4}$$

where $E_{\rm ref}$ is a reference energy and $\theta_{\rm ref}$ is a reference angle. Because the Rutherford formula can be separated into a factor that depends only on the energy and a factor that depends only on the scattering angle, $R=1$ for pure Rutherford scattering.

In our experiment $\theta_{\rm ref}$ is a forward angle (60°) and θ is a back angle (140°–160°). The reference energy is taken

to be 7 MeV, the lowest bombarding energy at which measurements were made. Since the main effect of the polarizability is to reduce the cross section at large angles and high energies, we expect that the measured values of R will be smaller than 1, and that the deviations from $R=1$ will increase as the bombarding energy E is increased.

Again following the procedure of Refs. 2 and 3, counting was done simultaneously at the angles θ and $\theta_{\rm ref}$, so that the bombarding energy and the integral of beam current times target thickness were identical for the two angles. Also, the target and detector setup was left undisturbed between runs at different energies so that detector angles and solid angles were unchanged. When the experiment is performed under these conditions, R can be simply obtained from

$$R(E,\theta)=\frac{N(E,\theta)}{N(E,\theta_{\rm ref})}\Big/\frac{N(E_{\rm ref},\theta)}{N(E_{\rm ref},\theta_{\rm ref})}\ , \qquad (5)$$

where $N(E,\theta)$ is the number of counts recorded at energy E and angle θ.

III. DESCRIPTION OF THE EXPERIMENT

A. Experimental details

The measurements were performed using a ^{3}He beam from the University of Wisconsin tandem Van de Graaff accelerator. The beam was defined by 1-mm-wide×1.5-mm-high slits placed 16.5 cm upstream from the target. A fast feedback system was used to keep the beam centered on the slits. The targets were composed of 99.4% enriched ^{208}Pb evaporated to a thickness of approximately 160 μg/cm^2 onto thin (5–10 μg/cm^2) C foils. Eight thin (250–300 μm) solid-state detectors were placed around the target in pairs at angles of 60°, 140°, 150°, and 160°. The field of view of each detector was restricted to a small area around the target by the use of collimators. All slits and collimators were made of thin (0.13 mm) Ta sheet to reduce slit-edge scattering. Small permanent magnets were used to prevent electrons from the target from reaching the detectors.

A sample detector pulse-height spectrum, obtained at $E=13$ MeV, $\theta=60°$, is shown in Fig. 1. In addition to the strong ^{208}Pb elastic-scattering peak, one sees smaller peaks from scattering and reactions on the ^{12}C in the target backing. For most energies and angles, these contaminant peaks were well resolved from the peak of interest. However, there were a few cases in which the peak from the ^{12}C(^{3}He,α)^{11}C reaction to the ground state of ^{11}C overlapped the Pb peak. To correct for this, separate runs were taken at each energy and angle with a blank carbon foil. The carbon spectra were then used to subtract the contaminations due to the carbon backing from the corresponding Pb target spectra. The resulting correction to the peak sum was usually less than 0.01%, although in a few instances corrections as large as 0.5% were required. In all cases, the statistical uncertainty in the correction to the peak sum was very small compared to the statistical uncertainty in the peak sum itself.

The method used to subtract the carbon contaminants

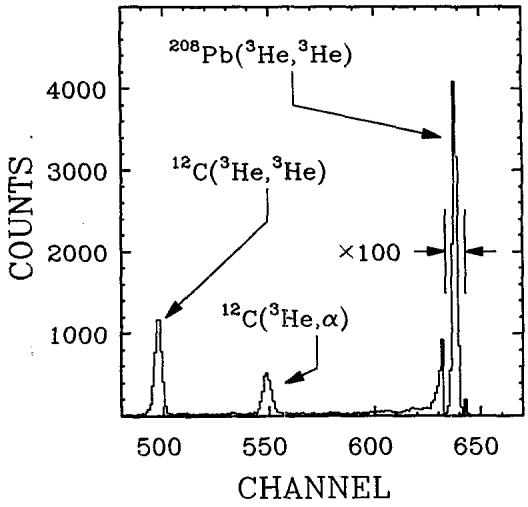

FIG. 1. A typical pulse-height spectrum obtained with $E=13$ MeV and $\theta=60°$. The dispersion is approximately 20 keV/channel.

is illustrated in Fig. 2, which shows the Pb and carbon spectra for $E=7$ MeV, $\theta=60°$. In this example the ^{12}C(^{3}He,α)^{11}C peak overlaps the ^{208}Pb elastic-scattering peak and must be subtracted. The proper normalization for the subtraction was determined by comparing the number of counts in carbon peaks which are well separated from the ^{208}Pb peak. The contaminant subtraction is complicated by the fact that the peaks in the Pb spectrum are slightly wider than the corresponding peaks in the C spectrum. To minimize the errors associated with this shape difference, the summation limits were always chosen so that the contaminant peak was either completely inside or completely outside the summation region.

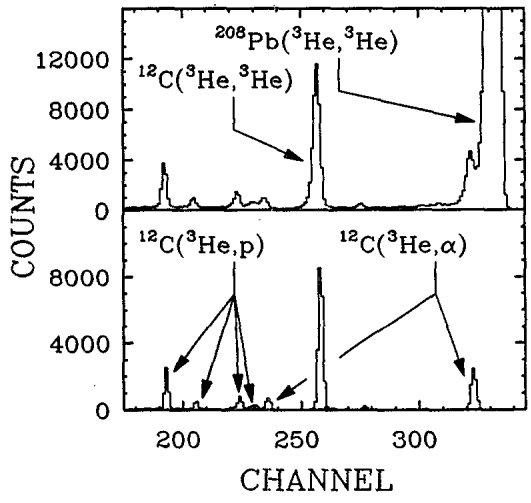

FIG. 2. Pulse-height spectra obtained with $E=7$ MeV and $\theta=60°$. The upper panel shows the spectrum for ^{208}Pb on a carbon backing, while the lower panel is for a carbon only target. The small peak near channel 278 is from ^{3}He elastic scattering from ^{16}O.

The effects of left-right motion of the beam spot on the target are effectively removed by the use of left-right symmetric detectors. The procedure we use is to calculate R separately for the left and right detectors, and then take the geometrical mean, $R=(R_l R_r)^{1/2}$. This eliminates beam motion errors to first order in Δx. We estimate that the residual error in R is less than 3 parts in 10^6.

Electronics dead times were kept low (typically less than 3%) and roughly equal for the various detector angles so that the resulting corrections to R were small (typically on the order of 0.1%).

In order to provide consistency checks, several experimental runs were made at each energy. The general pattern followed was to make a measurement at $E_{\rm ref}$ (7 MeV) followed by measurements at two or three higher energies. This cycle was repeated until the statistical accuracy desired at each energy was achieved. This technique not only allows for several independent determinations of R at each energy, but also heavily weights the statistics in favor of the 7-MeV reference data, since a measurement at the reference energy is made for each cycle. This is important, since each determination of R depends on information from the 7-MeV reference data. If Eq. (5) is rewritten as $R(E,\theta)=Q(E,\theta)/Q(7,\theta)$, where Q is given in terms of the corrected peak sums as $Q(E,\theta)=N(E,\theta)/N(E,60°)$, then it becomes clear that the ratios Q, which contain information from only a single energy, should be consistent over any number of runs at a given energy. The statistical uncertainties can then be reduced by calculating error-weighted averages for the ratios Q over all the independent measurements at a given energy.

Some modifications to the procedure described above were required for the measurements at 16 and 17 MeV. For these energies, thicker detectors (1000 μm) were used in order to stop the higher-energy ^{3}He. Since this involved changing the setup, it is not possible to directly compare these measurements with the measurements at the 7-MeV reference energy. Instead, measurements at a secondary reference energy of $E_{\rm ref}=14$ MeV were interspersed among measurements at 16 and 17 MeV and then these higher-energy data were referenced to the 7-MeV data using

$$R(E_{\rm ref}=7\ \text{MeV})=R(E=14\ \text{MeV},E_{\rm ref}=7\ \text{MeV}) \times R(E_{\rm ref}=14\ \text{MeV})\ . \quad (6)$$

Measurements of R at $E=15$ MeV were obtained using both the thin detectors and the thick detectors, and the values obtained in the two cases were consistent to within the statistical uncertainties. The contaminant corrections were small (less than 0.01%) for energies of 14 MeV and above.

B. Determination of the peak sums

One of the most critical aspects of this experiment is to ensure that the peak sums used in determining $R(E,\theta)$ are obtained in a uniform manner. As can be seen in Fig. 1, the elastic-scattering peaks have low-energy tails (presumably from slit-edge scattering), and since the number of counts in the tail region is significant, it is important to always include the same fraction of these counts in the peak sum. Several methods of summing the Pb peaks were tested and, in the end, the following relatively straightforward method was found to give consistent results for R. This method simply involves choosing a fixed width, W, for the summation region, and including in the peak sum the W channels adjacent to the peak with the largest number of counts. The consistency of the method was tested by extracting R for different choices of W. We found that, as a function of W, the value of R for each angle and energy was uniform over a large range. The final values of R were calculated using $W=24$ channels (the dispersion is about 20 keV/channel) which lies well inside the uniform region for all energies and angles.

Figure 3 shows the variation of R with W for $E=13$ MeV, $\theta=150°$. Here the open symbols correspond to the raw spectra (before the contaminant subtraction), while the filled symbols are for the corrected spectra. Note that as W is increased to include the main part of the peak, the values of R obtained with the corrected spectra approach a constant value. The results obtained from the uncorrected spectra are in good agreement with the results obtained from the corrected data for small values of W, but as W is increased the values of R begin to deviate as counts from contaminant peaks begin to be included in the peak sums. In particular, the increase in the extracted value of R (for the uncorrected spectra) from $W=12$ to 21 channels is caused by the ^{12}C(^{3}He,α)^{11}C peak shown in Fig. 2, while the subsequent decrease in R around $W=30$ is caused by another contaminant peak in the 7-MeV, 150° spectrum (not shown).

C. Multiple-scattering corrections

To minimize multiple-scattering effects, relatively thin targets (approximately 160 μg/cm^2) were used. In spite

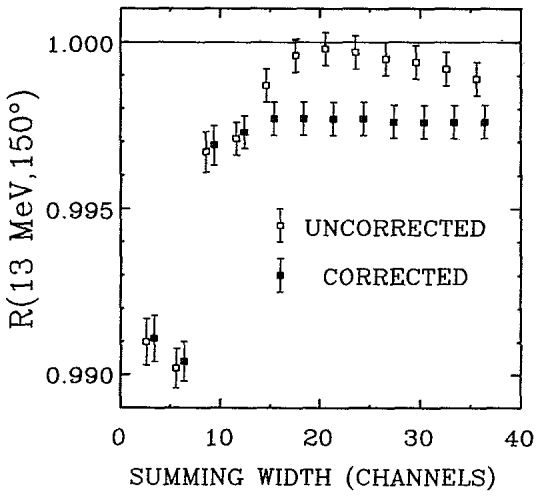

FIG. 3. Variation of R ($E=13$ MeV, $\theta=150°$) as a function of the number of channels included in each peak sum. The reference energy is 7 MeV and the reference angle is 60°.

of this it is still necessary to include a small correction for multiple scattering.

Conventional multiple-scattering calculations are clearly not adequate for our purposes since these calculations generally involve small-angle approximations and additional assumptions which are inappropriate for our experimental conditions. The approach we have used is to calculate the multiple-scattering corrections by simulating the scattering process with a Monte Carlo calculation. The single-scattering distribution used in this simulation was calculated from a screened Coulomb potential corresponding to the electron density distribution derived from a relativistic Hartree-Fock calculation[6] for Pb.

Special care was taken to properly account for events in which the projectile initially scatters through an angle close to 90°. For these events, the path length of the projectile inside the target material can be much longer than the target thickness and the probability of a second scattering is greatly enhanced. Events of this kind were discarded whenever the calculated energy loss was large enough to cause the event to fall outside the usual peak summation window. If this energy-loss criterion is not imposed, a substantial number of these events end up contributing to the count rate in the angle regions of interest.

According to the Monte Carlo calculations, the multiple-scattering corrections for our experimental conditions are dominated by double scattering. This result was verified by comparing the predicted multiple-scattering distribution from the full Monte Carlo calculations with a direct calculation (by numerical integration) of single scattering plus double scattering.

The Monte Carlo calculations at $E=7$ MeV predict that the net effect of the multiple scattering is to increase the ratio $N(E,60°)/N(E,150°)$ by $(3.1\pm1.1)\times10^{-4}$ compared to the expected result for pure single scattering. Here the quoted error represents the statistical uncertainty in the Monte Carlo calculation. Since the corrections are dominated by double scattering, we assume that the correction to $N(E,60°)/N(E,150°)$ scales with energy as $1/E^2$. The alternative of carrying out a full Monte Carlo calculation at each energy would require prohibitively large amounts of computer time.

IV. ANALYSIS

A. Results for R

The experimental results are presented in Fig. 4. The quantities shown are values of R corresponding to energies $E=8.5-17$ MeV and angles $\theta=140°$, 150°, and 160°. In each case we have used $E_{\rm ref}=7$ MeV, and $\theta_{\rm ref}=60°$. The error bars shown include the statistical uncertainty as well as the uncertainty in the corrections for dead time, multiple scattering, and carbon contaminant peaks. As expected, the measured values of R are near unity, and the deviations from $R=1$ become larger as the energy is increased. For $E\leq14$ MeV, R decreases rather slowly as a function of E, while for the higher energies the measured values fall off more rapidly.

The solid curve in Fig. 4 shows a calculation of $R(\theta=150°)$ for $\alpha=0.2$ fm^3. The purpose of this calculation is simply to illustrate the energy dependence which one would expect to obtain from the R^{-4} polarization potential (the calculation shown also includes small contributions that arise from atomic screening, vacuum polarization, and relativistic corrections). Since the energy dependence of the measurements is similar to the calculated curve for $E\leq14$ MeV, the most straightforward interpretation of the results is that for $E\leq14$ MeV the deviations from $R=1$ result primarily from electric polarization, while for $E\geq15$ MeV nuclear interactions between the ^{3}He and the ^{208}Pb nuclei begin to have a significant effect on R.

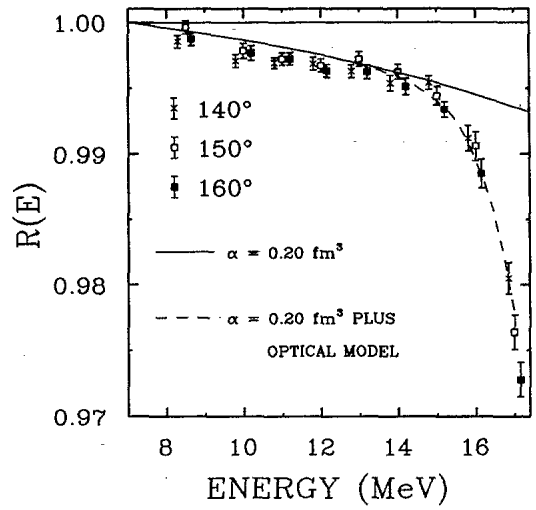

FIG. 4. Measurements of $R(E)$ for $E_{\rm ref}=7$ MeV, $\theta_{\rm ref}=60°$, and $\theta=140°$, 150°, and 160°. The solid curve shows the calculated effect of the electric polarizability of ^{3}He with $\alpha=0.2$ fm^3. This calculation also includes the effects of atomic screening, vacuum polarization, and relativistic corrections. The dashed line includes all of these same effects plus an estimate of the contribution from nuclear interactions. The curves are for $\theta=150°$.

Before attempting to extract a value of α from the measurements, this conjecture must be verified and a careful estimate of the size of the nuclear contribution to R at each energy must be determined. The methods we have used to do this are described in the following section.

B. Nuclear effects

Nuclear interactions can affect the elastic cross section in two ways. First, the long-range tail of the nuclear potential can alter the trajectories of the ^{3}He nuclei. Second, the existence of nuclear reactions can lead to the loss of flux from the elastic-scattering channel. The most direct means of estimating the nuclear contribution to the elastic-scattering cross section is with the optical model. Unfortunately, published optical-model-parameter sets[7–9] are unsuitable for our purposes, since they do an extremely poor job of describing the elastic-scattering process at low energies. In particular, we find that, for energies from 14 to 17 MeV, the existing potentials predict deviations from $R=1$ that are roughly 20 times

larger than the measured deviations. It appears that the problem with these potentials is that the predicted total reaction cross sections are much too large. The potentials of Refs. 7–9 were derived by fitting elastic-scattering data at ^{3}He energies of 20 to 217 MeV, and since the nuclear reaction mechanisms at these higher energies are qualitatively different from those at sub-Coulomb energies, it is not surprising that these potentials are inadequate for describing elastic scattering at lower energies. It is well known that the measurements at lower energies are sensitive mainly to the long-range tail of the nuclear potential whereas those at higher energies are relatively insensitive to this feature of the potential.

In order to obtain an optical-model potential that gives more reasonable results at low energies it was necessary to adjust the parameters used in the optical model. Beginning with the potential from Ref. 7, the real and imaginary diffuseness parameters were adjusted to fit our data at energies between 15 and 17 MeV. The dashed curve in Fig. 4 shows the predictions obtained for R ($\theta=150°$) from the resulting potential. This calculation includes the contributions from the polarization potential (again with $\alpha=0.2$ fm^3) as well as contributions from the nuclear potential.

While this calculation suggests that the measurements for $E \leq 14$ MeV are essentially free of nuclear effects, one cannot rule out the possibility that some different set of optical-model parameters would predict a qualitatively different behavior for the low-energy cross sections. For this reason, we have carried out additional calculations aimed at determining the size of the nuclear contributions. The basic idea of these calculations is to focus on the energy dependence of various processes that can affect $R(E)$. Then, by combining information about the energy dependence with the fact that the net effect of the nuclear interactions at $E=17$ MeV is no more than 2–3 % (see Fig. 4), we can set an upper limit on the size of the nuclear contribution at lower energies.

As noted earlier, one of the important effects is the loss of flux into reaction channels. For sub-Coulomb energies, reactions occur mainly for projectiles which have small impact parameters, and therefore the effect of the loss of flux is to reduce the back angle elastic-scattering cross section. To a good approximation, the net decrease in the elastic-scattering cross section (integrated over the back angles) is just equal to the total reaction cross section. It follows that the energy dependence of $R(E)$ should be determined by the energy dependence of the dominant reaction cross sections.

We have carried out a series of reaction calculations, using distorted-wave Born approximation (DWBA) and classical Coulomb excitation theory, for a variety of ^{3}He+^{208}Pb reaction channels. In Fig. 5 we show the calculated energy dependence of the total reaction cross section, normalized to 1 at $E=17$ MeV, for several reaction channels. The solid curves are for (^{3}He,d) reactions leading to final states in ^{209}Bi, and the dashed curves are for (^{3}He,α) reactions. The dotted curve shows the cross section for Coulomb excitation of the 3^- state in ^{208}Pb, while the dot-dashed curve is for Coulomb breakup of ^{3}He into $d+p$. What these calculations show is that, except for the inelastic scattering to the 3^- state, all of the reaction cross sections have a very strong energy dependence, typically dropping by a factor of 3 or more for each 1-MeV decrease in the bombarding energy.

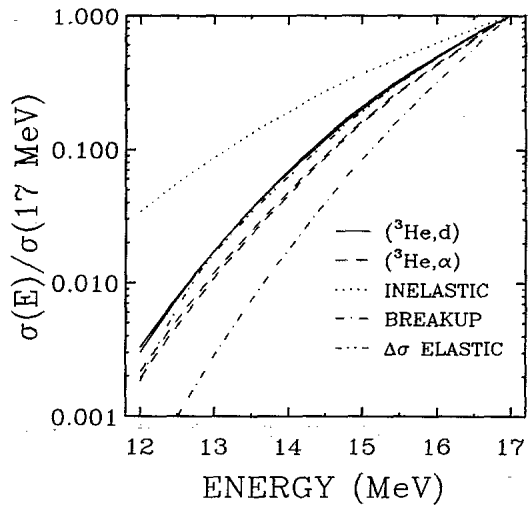

FIG. 5 Calculated energy dependence of cross sections of several strong nuclear processes. The quantity $\Delta\sigma$ elastic is defined in the text.

Of all the processes investigated, only inelastic scattering to the 3^- state in ^{208}Pb fails to exhibit this strong energy dependence. Fortunately, for this particular reaction channel one can reliably calculate the absolute magnitude of the cross section as well as its energy dependence, since the $B(E3)$ value of the transition is known. The result is that even for our highest energy (17 MeV) the differential cross section for the inelastic scattering is smaller than the elastic cross section by a factor of 10^4. In fact, at the appropriate energy in the 17-MeV spectra we see evidence of a very small peak of about this magnitude. We conclude that inelastic scattering to the 3^- state should have a negligible effect on $R(E)$ (less than 1×10^{-4}) for energies below 17 MeV.

The calculations described so far provide information about the energy dependence of the reaction processes. It is also important to investigate the energy dependence of any contributions to $R(E)$ that arise from the real part of the nuclear potential. This has been done by carrying out optical-model calculations for a set of potentials in which the parameters of the real central well were adjusted to make large changes in the tail of the potential (in the region near the classical turning point) while keeping the total reaction cross section fixed. This allows us to separate effects caused by absorption from those caused by the real potential. The quantity of interest is the difference in the calculated elastic-scattering cross sections (at $\theta=150°$), $\Delta\sigma=\sigma_1-\sigma_2$, where σ_1 (σ_2) corresponds to a parameter set for which the real potential is relatively strong (weak). The presumption here is that since the two calculations have the same reaction cross section, the absorption effects should be comparable in the two cases, and consequently $\Delta\sigma$ should be a measure of the effect of the real potential. We are primarily in-

terested in the energy dependence of $\Delta\sigma$, which is shown by the dash-dot-dotted curve in Fig. 5 (as before, $\Delta\sigma$ is normalized to 1 at 17 MeV). We find that the effect of the real potential also has a strong energy dependence, similar to that of most of the reaction channels.

Based on the calculations shown in Fig. 5, it is reasonable to conclude that the nuclear contribution to R should decrease in magnitude by about a factor of 3 for each 1-MeV decrease in the energy. This conclusion appears to be consistent with the observed behavior of $R(E)$. In particular, we note that in Fig. 4, the measured values of R from 15 to 17 MeV show a strong energy dependence, with the size of the apparent nuclear contribution falling by roughly a factor of 3 per MeV. Assuming that this trend continues to the lower energies, the nuclear contribution to R will be less than 0.1% at 14 MeV and will be negligible for $E \leq 13$ MeV.

C. Determination of α

On the basis of the calculations described above, we conclude that the measurements for $E \leq 14$ MeV can be used to extract an experimental value for α. At 14 MeV it is necessary to make a small correction for the nuclear contribution, and this has been done by making use of the optical-model calculation shown in Fig. 4. The uncertainty in the correction is assumed to be equal to the size of the correction itself; i.e., the correction for nuclear interactions is taken to be 0.0005 ± 0.0005.

Several other effects also give rise to small changes in the elastic-scattering cross section at low energies. These effects, which include atomic screening, vacuum polarization, and relativistic corrections, are well understood and readily calculated.[2] Although together these effects can change the cross section by as much as 3%, their effect on R is less than 0.05%. The combined effect of these three processes is indicated by the dashed curve in Fig. 6. Finally, it is necessary to include a small correction for the potential which arises from the electric polarization of the ^{208}Pb nucleus. If $\alpha_{\rm Pb}$ represents the polarizability of the ^{208}Pb nucleus, then the full polarization potential is given by

$$V_{\rm pol} = -\tfrac{1}{2}(Z^2\alpha + z^2\alpha_{\rm Pb})e^2/R^4 , \quad (7)$$

where Ze and ze are the charges of the ^{208}Pb and ^{3}He nuclei, respectively. For heavy nuclei the polarizability can be estimated[1] from the location of the giant dipole resonance, and the result for ^{208}Pb is $\alpha_{\rm Pb}=26$ fm^3. Since z is much smaller than Z, the ^{208}Pb polarization term in Eq. (7) represents a small (about 6%) correction to α. The solid curve in Fig. 6 shows our final calculation in which the value of alpha has been adjusted to fit the data for $E \leq 14$ MeV. This calculation includes the corrections for nuclear effects as well as for atomic screening, vacuum polarization, relativistic effects, and polarization of the ^{208}Pb nucleus. In fitting the data and extracting the uncertainty in α, we have taken into account the fact that the errors in the individual measurements of R are correlated. Our final result for the electric polarizability of the ^{3}He nucleus is

$$\alpha = 0.250\pm0.040 \text{ fm}^3 . \quad (8)$$

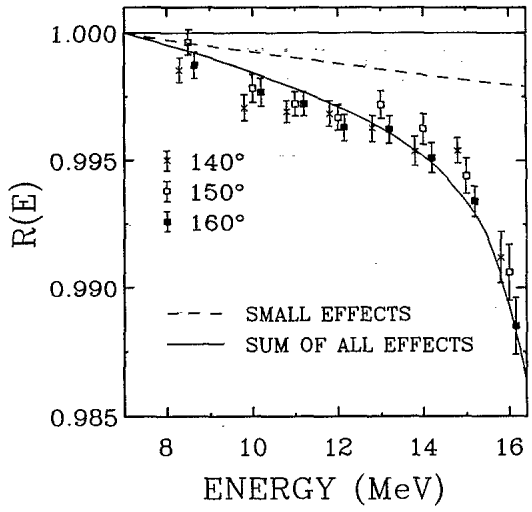

FIG. 6. Measurements of $R(E,\theta)$ for $E \leq 16$ MeV, with $E_{\rm ref}=7$ MeV, $\theta_{\rm ref}=60°$. The dashed curve shows the combined effect of atomic screening, vacuum polarization, and relativistic corrections. The solid curve shows the sum of these processes plus nuclear interactions and electric polarizations, with $\alpha=0.250$ fm^3 and $\alpha_{\rm Pb}=26$ fm^3.

The error we quote for α is dominated by the statistical uncertainty in the measured values of R, but also reflects our estimate of the uncertainty in the nuclear correction and the ^{208}Pb polarizability.

V. DISCUSSION

The electric polarizability is related in a simple way[1,5] to the ^{3}He photoabsorption cross section, $\sigma(E)$:

$$\alpha = (\hbar c/2\pi^2)\sigma_{-2}(E1) , \quad (9)$$

where

$$\sigma_{-2} = \int_0^\infty E^{-2}\sigma(E)dE , \quad (10)$$

and $\sigma_{-2}(E1)$ is the electric dipole part of σ_{-2}. There have been several independent measurements of the total cross sections for both the two-body and three-body photodisintegration of ^{3}He. Cross-section measurements for the two-body process, ^{3}He$(\gamma,d)^1$H, obtained in a number of different experiments are compiled in Ref. 10. Overall, the agreement between the various measurements is quite good, with differences of typically no more than 25%. There have also been several measurements of the cross section for three-body photodisintegration. In this case the discrepancies are somewhat larger (see, for example, Fig. 9 of Ref. 11), but at the peak of the cross section the agreement between the various measurements is good.

From the measurements shown in Refs. 10 and 11, it is straightforward to evaluate the energy-weighted sum in Eq. (10). Depending on the choice of data set, we obtain results in the range $\sigma_{-2}=0.13$ to 0.17 mb/MeV. Neglecting the non-$E1$ contributions to σ_{-2}, this corresponds to polarizabilities of $\alpha=0.13$ to 0.17 fm^3.

We know of no satisfactory explanation for the discrepancy between our measurement of α and the result

derived from the photodisintegration cross sections. In the calculation of σ_{-2} there are roughly equal contributions from two-body and three-body breakup, and in view of the fact that both processes have been measured several times, it seems unlikely that these measurements could be in error by enough to cause the observed discrepancy. On the other hand, we are confident that our own cross-section measurements are reliable.

To our knowledge, there have been no direct theoretical calculations of the ^{3}He polarizability. However, there have been several calculations of the photoabsorption cross sections (see, for example, Refs. 12–15). Generally speaking, the calculated cross sections tend to be somewhat larger in magnitude than the corresponding measurements, but the difference does not appear to be sufficient to make up the discrepancy between our measurement of α and the experimental σ_{-2} result. While these results suggest that the theoretical prediction for α would be somewhat smaller than our measurement, we believe that a new calculation of the ^{3}He polarizability using modern Faddeev wave functions for both the bound and continuum states would be valuable.

ACKNOWLEDGMENTS

We would like to thank Nathan Rodning for his contributions during the early stages of this experiment. We are also indebted to Professor W. Lynch for detecting an error in our calculation of the relativistic corrections. This work was supported in part by the National Science Foundation under Grant No. PHY-8717764.

[1]G. Baur, F. Roesel, and D. Trautmann, Nucl. Phys. **A288**, 113 (1977).
[2]W. G. Lynch, M. B. Tsang, H. C. Bhang, J. G. Cramer, and R. J. Puigh, Phys. Rev. Lett. **48**, 979 (1982).
[3]N. L. Rodning, L. D. Knutson, W. G. Lynch, and M. B. Tsang, Phys. Rev. Lett. **49**, 909 (1982).
[4]D. Vetterli *et al.*, Phys. Rev. Lett. **62**, 1453 (1989).
[5]T. E. O. Ericson and J. Hüfner, Nucl. Phys. **B47**, 205 (1972).
[6]A. D. McLean and R. S. McLean, At. Data Nucl. Data Tables **26**, 197 (1981).
[7]C. M. Perey and F. G. Perey, At. Data Nucl. Data Tables **17**, 1 (1976).
[8]S. M. Barr and R. M. DelVecchio, Phys. Rev. C **15**, 114 (1977).
[9]A. Djaloeis, J.-P. Didelez, A. Galonsky, and W. Oelert, Nucl. Phys. **A306**, 221 (1978).
[10]G. Ticcioni, S. N. Gardiner, J. L. Matthews, and R. O. Owens, Phys. Lett. **46B**, 369 (1973).
[11]D. D. Faul, B. L. Berman, P. Meyer, and D. L. Olson, Phys. Rev. C **24**, 849 (1981).
[12]I. M. Barbour and A. C. Phillips, Phys. Rev. C **1**, 165 (1970).
[13]B. F. Gibson and D. R. Lehman, Phys. Rev. C **11**, 29 (1975).
[14]B. F. Gibson and D. R. Lehman, Phys. Rev. C **13**, 477 (1976).
[15]J. S. Levinger and R. Fitzgibbon, Phys. Rev. C **18**, 56 (1978).